Direct Measurement of Friction of a Fluctuating Contact Line

Shuo Guo,[1] Min Gao,[2] Xiaomin Xiong,[1,3] Yong Jian Wang,[1] Xiaoping Wang,[2] Ping Sheng,[1] and Penger Tong[1]

[1]*Department of Physics, Hong Kong University of Science and Technology, Clear Water Bay, Kowloon, Hong Kong*
[2]*Department of Mathematics, Hong Kong University of Science and Technology, Clear Water Bay, Kowloon, Hong Kong*
[3]*Department of Physics and State Key Laboratory of Optoelectronic Materials and Technologies, Sun Yat-sen University, Guangzhou 510275, China*

(Received 22 January 2013; revised manuscript received 25 April 2013; published 10 July 2013)

We report a direct measurement of the friction coefficient of a fluctuating (and slipping) contact line using a thin vertical glass fiber of diameter d with one end glued onto a cantilever beam and the other end touching a liquid-air interface. By measuring the broadening of the resonant peak of the cantilever system with varying liquid viscosity η, we find the friction coefficient of the contact line has a universal form, $\xi_c \simeq 0.8\pi d\eta$, independent of the liquid-solid contact angle. The obtained scaling law is further supported by the numerical simulation based on the phase field model under the generalized Navier boundary conditions.

DOI: 10.1103/PhysRevLett.111.026101 PACS numbers: 68.08.−p, 05.40.−a, 83.50.Lh, 83.85.Vb

What happens near a contact line, where a liquid interface between two (immiscible) fluids intersects with a solid surface is a fundamental issue in fluid dynamics and is also a concern of many industrial processes ranging from spreading of droplets, lubricants, and coatings to the extraction of oil from sandstone by injecting water or gas [1]. While considerable progress has been made recently in controlling the wettability of various textured solid surfaces [2] and in understanding the energetics associated with deformable soft substrates [3–5], our fundamental understanding of the dynamics of the contact line still remains very limited [1,6]. Like the static problem [3–5], the motion of the contact line is also a singular problem; it is incompatible with the nonslip boundary condition and would lead to unphysical infinite dissipation [7]. Over the years there have been many *ad hoc* models and proposals aimed at resolving the incompatibility issue [1,2,6], but none of the theoretical ideas has been experimentally confirmed.

As illustrated in the inset of Fig. 1, a moving contact line (MCL) involves fluid motion (i) at a small distance a (~ 1 nm) in the immediate vicinity of the contact line, in which molecular interactions between the liquid and solid are important, and (ii) in the "outer region" of meso- or macroscopic size ℓ, in which classical hydrodynamics are applicable. To avoid the dissipation divergence of MCL, de Gennes *et al.* [8] introduced the cutoff length a and calculated the hydrodynamic friction coefficient ξ_w in regime (ii) away from the contact line,

$$\xi_w \simeq [3\ln(\ell/a)/\theta]\pi d\eta, \tag{1}$$

for liquids with a small contact angle θ. In the above, πd is the contact line length, and η is the fluid viscosity. The value of ξ_w becomes very large for liquids with small θ and even becomes divergent when $\theta = 0°$.

Most experiments on MCL were conducted in regime (ii) [9–11], because direct observation of the fluid motion in regime (i) ($\lesssim 1$ μm) is difficult with the conventional optical methods. While these measurements provided useful information about the MCL dynamics at large distances, direct comparison of the experimental results with the microscopic models is not possible. This is because all the theories predicted the same flow field to the leading order [1,12,13]. As a result, our current understanding of the contact line dynamics in regime (i) relies mainly on the results from molecular dynamic (MD) simulations [14–16]. These simulations, however, were carried out under highly idealized conditions, such as atomically smooth solid surface and simplified fluid-solid interactions. Direct measurement of the properties of the MCL in regime (i) is, therefore, needed in order to test different theoretical ideas.

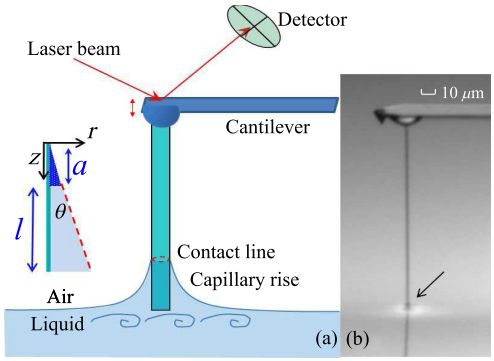

FIG. 1 (color online). (a) Sketch of the AFM-based hanging fiber probe and the capillary rise around the fiber tip. Inset shows the geometry near the contact line and the coordinate system used in the experiment. (b) Actual glass fiber of diameter $d = 1.9$ μm and length 270 μm in contact with a decane-air interface. The arrow points to the contact point.

In this Letter, we report direct measurement of the scaling properties of the friction coefficient ξ_c of the MCL in regime (i) through the measurement of the spectrum of fluctuation amplitude of a contact line at equilibrium (no external driving), which is amplified under the spontaneous resonance condition. The two quantities are intrinsically linked together by the fluctuation-dissipation theorem [17], which establishes what happens at the microscopic level to a macroscopically measurable dissipation coefficient.

Figure 1 shows the working principle and the actual setup of a newly developed hanging fiber resonator [18] based on atomic force microscopy (AFM). A vertical glass fiber of diameter in the range of 0.4–2.5 μm and length in the range 130–300 μm is glued onto the further end of a rectangular AFM cantilever beam. The tip of the hanging fiber touches a liquid-air interface, at which a circular contact line between the interface and the fiber surface is formed. The vertical displacement $z(t)$ of the fiber ($\equiv$ vertical deflection of the AFM cantilever) is well described by the Langevin equation [18,19]:

$$m\frac{\partial^2 z}{\partial t^2} + \xi\frac{\partial z}{\partial t} + kz = f_B(t), \tag{2}$$

where m is the effective mass of the modified cantilever, $\xi\partial z/\partial t$ is the drag force on the fiber with ξ being the friction coefficient, $kz(t)$ is the elastic force due to the bending of the cantilever with a spring constant k, and $f_B(t)$ is the random Brownian force due to thermal fluctuations of the surrounding fluid. While $f_B(t)$ has a zero mean, its rms value, $\langle f_B^2\rangle = 2k_BT\xi$, is a nonzero quantity with k_BT being the thermal energy of the system.

The measured quantity in the experiment is the power spectrum of vertical deflections of the cantilever, $|z(\omega)|^2$, which can be solved analytically from Eq. (2):

$$|z(\omega)|^2 = \frac{2k_BT\xi/m^2}{(\omega^2 - \omega_0^2)^2 + (\omega\xi/m)^2}, \tag{3}$$

where $\omega = 2\pi f$ is the angular frequency and $\omega_0 = (k/m)^{1/2}$ (~ 600 kHz) is the resonant frequency of the hanging fiber. Being operated at a resonant state, the hanging fiber amplifies the fluctuation spectrum and thus can accurately detect minute changes of the friction coefficient ξ caused by the damping of a spontaneously fluctuating contact line [20].

The setup in Fig. 1 has several features particularly useful for the investigation intended here. (i) When the fiber tip touches the liquid interface, the resulting capillary force on the fiber is immediately detected by the AFM force sensor, making the determination of the contact point very accurate to within 0.1 μm. By pulling the fiber upward slightly to keep the fiber tip in minimal contact with the liquid interface, the drag force from the bulk fluid is minimized. (ii) By pushing downward and pulling upward the fiber through the liquid interface, one can immediately measure the advancing and receding contact angles resulting from the interfacial pinning. These real-time measurements ensure that the cleaned fiber surface and liquid interface are kept under an equilibrium condition.

(iii) As indicated in Fig. 1, there is a small capillary rise of the wetting fluid around the fiber. The meniscus of the interface around a stationary fiber has the form [8], $r(h) = b\cosh[h/b - \ln(2\ell_c/b)]$, where h is the meniscus height, r is its radial location, $\ell_c = \sqrt{\gamma/\rho g}$ is the capillary length, and $b = (d/2)\cos\theta$. Here, γ is the surface tension, ρ is the fluid density, g is the gravitational acceleration, and d is the fiber diameter. In this case, we have a capillary rise of $\sim 3d$ in height and $\sim 1.5d$ in film thickness. When the fiber oscillates, the viscous shear wave can only penetrate into a thin fluid layer of thickness $\delta = (2\nu/\omega_0)^{1/2}$ from the fiber surface [21], where $\nu = \eta/\rho$ is the kinematic viscosity. The capillary rise [i.e., the fluid in regime (ii) marked as a wedge-shaped fluid layer in the inset of Fig. 1(a)] will oscillate in phase with the fiber, contributing only an added mass and no dissipation to the oscillating fiber, if its thickness is smaller than δ. For liquids with $\eta \gtrsim 1$ cP and $\omega_0 \simeq 2\pi \times 110$ kHz, we have $\delta \gtrsim 1.7$ μm. By choosing the glass fibers with $d \lesssim 2$ μm, we deliberately minimize the viscous drag from the capillary rise around the fiber and thus avoid the dissipation divergence at the zero contact angle limit [see Eq. (1)]. The above discussion is valid only for the fluid layer with a nonslip boundary condition [i.e., in regime (ii)]. As a result, the oscillating fiber only feels the drag on its end surface and the MCL in regime (i), where the wall velocity slips as demonstrated by previous MD simulations [14–16] and by recent continuum hydrodynamic calculations [16,22,23]. Such a slip produces a relative motion between the contact line and the fiber.

Figure 2 shows how the measured $|z(f)|^2$ changes when the fiber tip ($d = 2$ μm) touches the liquid-air interface with different viscosities. Nine organic liquids and aqueous solutions of glycerine are used in the experiment and their properties are given in [20]. These liquid samples are chosen because their interfacial properties are stable and a wide range of viscosities is covered. Once in contact with the interface, the resonant peak changes continuously with increasing fluid viscosity η; the frequency peak broadens while the peak height decreases and peak position shifts to lower frequencies. This behavior is well described by Eq. (3), as shown by the fitted solid line in the inset of Fig. 2. From the equipartition theorem, one finds the measured rms value of contact line fluctuations to be $\langle z^2(t)\rangle_t^{1/2} = (k_BT/k)^{1/2} \simeq 2 \times 10^{-2}$ nm for $k = 10$ N/m. The corresponding drag force is $f_d \simeq \xi\omega_0\langle z^2(t)\rangle_t^{1/2} \simeq 1$ pN and the capillary number $Ca \simeq \eta\omega_0\langle z^2(t)\rangle_t^{1/2}/\gamma \simeq 1.9 \times 10^{-7}$ for water with $\xi = 10^{-7}$ Ns/m and $\omega_0 = 2\pi \times 110$ kHz. These numbers reveal the tremendous sensitivity of the technique useful for the study of the MCL dynamics.

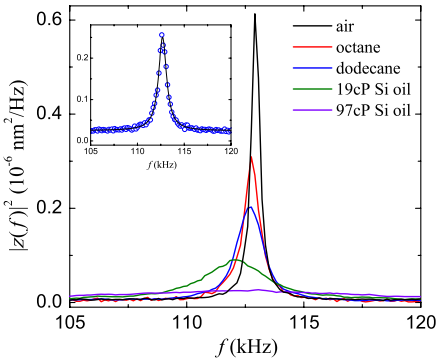

FIG. 2 (color online). Variations of the measured $|z(f)|^2$ when the fiber tip touches different fluids: air (black curve), octane (red curve), dodecane (blue curve), silicone oil 1 ($\eta = 19$ cP) (green curve) and silicone oil 2 ($\eta = 97$ cP) (violet). Inset shows a fit of Eq. (3) to the dodecane data with $m = 2.26 \times 10^{-8}$ g, $k = 11.33$ N/m, and $\xi = 8.28 \times 10^{-8}$ N s/m.

We also measure $|z(f)|^2$ when the fiber is in air and obtain the corresponding friction coefficient ξ_0. The net friction coefficient is then defined as $\Delta\xi \equiv \xi - \xi_0$, which is shown in Fig. 3(a) as a function of liquid viscosity η. Two sets of data obtained by using two different fibers are displayed. The error bars show the standard deviation of the repeated measurements. The overall uncertainties of the measured $\Delta\xi$ are at the 10% level. For the $d = 0.4$ μm fiber, the signals at the two lowest values of η have become very close to the noise floor (in air). The two sets of data can be well described by the equation,

$$\Delta\xi = A + \alpha\pi d\eta + \xi_b, \tag{4}$$

where A and α are two fitting parameters, and ξ_b is the friction coefficient resulting from the end surface of the fiber tip. For an oscillating disk fully immersed in an unbounded liquid of density ρ, its friction coefficient parallel to the normal of the disk is given by [24,25],

$$\xi_b = 4d\eta + \frac{8\sqrt{2}}{3\pi} d^2 \sqrt{\rho\omega_0\eta}, \tag{5}$$

where ω_0 is the oscillation frequency. Because the fiber has only one (circular) end surface in contact with the liquid, here we express ξ_b for only a half of its total value.

The solid lines in Fig. 3(a) show the fits to Eq. (4). The η-independent term A is a device parameter, which characterizes the internal dissipation of the hanging fiber under the capillary force. By varying η for more than two decades, we are able to accurately determine the linear term in η, which becomes dominant at large values of η, and the $\sqrt{\eta}$ term in ξ_b, which is more important at small values of η. It is found that the measured $\Delta\xi$ for different fibers with various values of d and ω_0 can all be described by Eq. (4). The frequency-dependent $\sqrt{\eta}$ term in Eq. (5), therefore, provides a unique way to separate the end effect from the measured $\Delta\xi$.

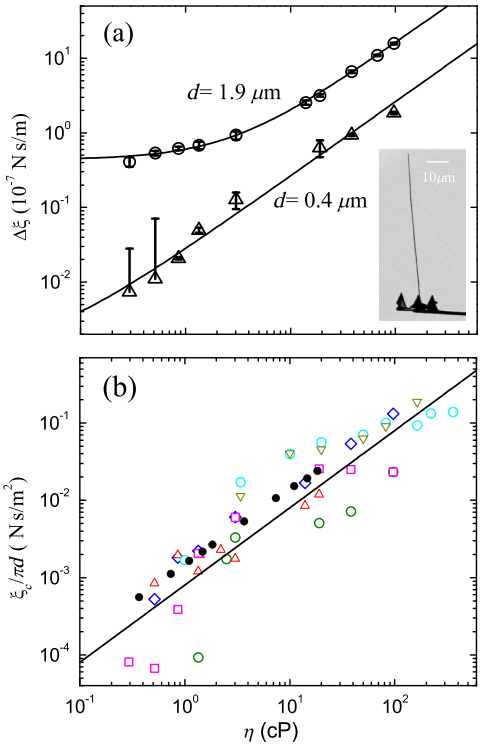

FIG. 3 (color online). (a) Measured $\Delta\xi$ as a function of liquid viscosity η. Two hanging fibers with (i) $d = 1.9$ μm, $k = 11$ N/m (circles) and (ii) $d = 0.4$ μm, $k = 9$ N/m (triangles) are used. Inset shows an SEM image of the $d = 0.4$ μm fiber. The solid lines show the fits to Eq. (4). (b) Measured $\xi_c/(\pi d)$ as a function of η. Six fibers are used: (i) $d = 2.3$ μm (green circles), (ii) $d = 2.1$ μm (red triangles), (iii) $d = 1.9$ μm (blue diamonds), (iv) $d = 0.4$ μm (magenta squares), (v) $d = 0.8$ μm (cyan circles), and (vi) $d = 2.1$ μm (yellow triangles). The solid line is a linear fit to Eq. (6) with $\alpha = 0.8 \pm 0.2$. The black solid circles are the simulation results obtained at $\theta = 30°$.

Once subtracting out the end contribution ξ_b and the device constant A, we find that the resulting friction coefficient, $\xi_c \equiv \Delta\xi - A - \xi_b$, for different fibers with varying diameters d (and hence varying capillary rises) and resonant frequencies ω_0 and for fluids with different contact angles θ all collapses into a single master curve. Figure 3(b) shows the obtained friction coefficient per unit length, $\xi_c/(\pi d)$, as a function of η. The first four sets of data are obtained using organic liquids, which show zero contact angle with the glass fiber. The last two sets of data are obtained using aqueous solutions of glycerine with various concentrations. In one case (v), the glass fiber is plasma cleaned and the contact angle is zero. In the other case (vi), the glass fiber is coated with a monolayer of trichloro(1H, 1H, 2H, 2H-perfluorooctyl)silane (FTS) and the (advancing) contact angle is changed from 0° to 100°. Such an increase in the contact angle also introduces a large contact angle hysteresis. Nevertheless, all the data sets can be well described by a universal function

$$\xi_c = \alpha \pi d \eta, \quad (6)$$

where πd is the total length of MCL and the fitted value of $\alpha = 0.8 \pm 0.2$ (solid line).

Loewenberg [26] has carried out a numerical study of the friction coefficient ξ for an oscillating cylinder of varying aspect ratio Γ fully immersed in an unbounded fluid (without a contact line). His numerical results indicated that the use of Eq. (5) to correct the end-wall effect is accurate and the numerical errors associated with the end-wall subtraction are negligibly small compared with the measured ξ_c shown in Fig. 3(b) [27].

The calculated ξ_w in Eq. (1) is $\xi_w \simeq (26/\theta)\pi d\eta$ for $\ell \simeq 6$ μm. This value of ξ_w is about 100 times larger than the measured ξ_c for liquids with $\theta \simeq 15°$ and even becomes divergent for liquids with $\theta = 0°$. Clearly, the calculated ξ_w for regime (ii) does not apply to the measured ξ_c shown in Fig. 3(b), further confirming that the capillary rise in regime (ii) does not contribute to the measured ξ_c. The direct comparison between the data sets (v) and (vi) with the same fluid but different fiber surfaces (hydrophilic vs hydrophobic) reveals that the measured ξ_c is insensitive to the changes of the contact angle and to the contact line pinning, as the measurement is conducted at equilibrium without involving a macroscopic flow.

In a more recent experiment, we measured ξ_c for the hanging fiber intersecting with a thin soap film [28]. In this case, there are two contact lines formed on the fiber surface (with the two water-air interfaces of the soap film) and no end-wall correction is needed. The measured ξ_c is found to decrease with time as the water in the soap film gradually drains out and reaches an asymptotic value when the film thickness becomes very small ($\lesssim 36$ nm) before the soap film bursts. The obtained asymptotic value of ξ_c is twice as large as the value given by Eq. (6). The universal behavior of the measured ξ_c for different fluid systems with various contact angles and capillary rises (by varying d) thus demonstrates that ξ_c given in Eq. (6) is indeed associated with a fluctuating (and slipping) contact line in regime (i).

In fact, ξ_c is an intrinsic property of the MCL and can also be realized through a macroscopic flow. To further verify this effect, we conduct a direct numerical simulation (DNS) of a two-dimensional two-phase (fluid and gas) flow between two parallel plates under a constant speed U_0 and the third dimension of the flow parallel to the contact line is assumed to be homogeneous [29]. The DNS study is carried out by solving the phase field model of coupled incompressible Navier-Stokes equation and Cahn-Hilliard equation under the generalized Navier boundary conditions using a gradient stable scheme [23,30]. From the obtained tangential velocity profile $v_x(x)$ at the solid wall as a function of distance x away from the contact line, where the x axis is along the flow direction, we compute the dissipation rate per unit length $\epsilon_u = (\eta/\ell_s)\int v_x^2(x)dx$, occurring at the fluid-solid interface, where the slip length ℓ_s ($= 10$ nm) is a fixed input parameter. The friction coefficient per unit length is ϵ_u/U_0^2, and from Eq. (6) we have $\alpha = \int [v_x(x)/U_0]^2 d(x/\ell_s)$. It is found that the normalized wall velocity $v_x(x)/U_0$ is a scaling function of x/ℓ_s, which slips mainly in the core region $x/\ell_s \lesssim 8$ and has a partial slip region with $v_x(x)/U_0 \sim \ell_s/x$ for all fluids with varying viscosities from 0.37 to 18.4 cP. [The calculated $v_x(x)$, as shown in Fig. 2 in [29], thus represents a velocity profile of the MCL in regime (i)].

The (black) solid circles in Fig. 3(b) are the calculated $\xi_c/(\pi d)$ at $\theta = 30°$. Each value of $\xi_c/(\pi d)$ is obtained by integrating the dissipation rate $(\eta/\ell_s)v_x^2(x)$ over the core region $x/\ell_s \leq 8$. As shown in [27], the smallest amplitude fluctuations detectable by the hanging fiber probe is set by the root mean vibration amplitude of the solid atoms. This lower cutoff length in fluid motion gives rise to a cutoff slip velocity $v_c \simeq 0.38U_0$, which occurs at a distance very close to $x/\ell_s \simeq 8$ and marks the onset of the $1/x$ regime. Therefore, the dissipation in the partial slip region and beyond is too small to be detected by the hanging fiber. Figure 3(b) clearly reveals that the numerical results are in good agreement with the measured $\xi_c/(\pi d)$.

The establishment of the direct connection between the measured ξ_c in Eq. (6) and the fluctuating (and slipping) contact line has several important implications. First, Eq. (6) as a universal scaling law applicable to liquids with different viscosities and contact angles establishes a rigorous relationship which can be used to test various microscopic models for MCL. Second, Eq. (6) sets up an intrinsic bound for the dissipation of the MCL in regime (i), which is useful for evaluating relevant molecular parameters associated with the MCL, such as ℓ_s for different fluids. Finally, the understanding of contact line dissipation also provides a solid foundation for the further study of other liquid interfaces of practical interest, such as those coated with polymers, surfactant and lipids.

We have benefited from illuminating discussions with T.-Z. Qian and E. Charlaix. This work was supported by RGC of Hong Kong SAR under Grants No. HKUST 603709 (P. T.), No. 605311 (X. W.), No. 604211 (P. S.), and No. SRFI11/SC02 (P. S.).

[1] D. Bonn, J. Eggers, J. Indekeu, J. Meunier, and E. Rolley, Rev. Mod. Phys. **81**, 739 (2009).
[2] D. Quéré, Annu. Rev. Mater. Res. **38**, 71 (2008).
[3] E. R. Jerison, Y. Xu, L. A. Wilen, and E. R. Dufresne, Phys. Rev. Lett. **106**, 186103 (2011).
[4] A. Marchand, S. Das, J. H. Snoeijer, and B. Andreotti, Phys. Rev. Lett. **109**, 236101 (2012).
[5] R. W. Style, R. Boltyanskiy, Y. Che, J. S. Wettlaufer, L. A. Wilen, and E. R. Dufresne, Phys. Rev. Lett. **110**, 066103 (2013).
[6] L. Leger and J.-F. Joanny, Rep. Prog. Phys. **55**, 431 (1992).
[7] E. B. V. Dussan and S. H. J. Davis, J. Fluid Mech. **65**, 71 (1974).

[8] P.-G. de Gennes, F. Brochard-Wyart, and D. Quere, *Capillarity and Wetting Phenomena* (Springer, New York, 2004).
[9] T. Ondarcuhu and M. Veyssié, Nature (London) **352**, 418 (1991).
[10] J. A. Marsh, S. Garoff, and V. E. B. Dussan, Phys. Rev. Lett. **70**, 2778 (1993).
[11] Q. Chen, E. Raméand, and S. Garoff, J. Fluid Mech. **337**, 49 (1997).
[12] E. B. V. Dussan, Annu. Rev. Fluid Mech. **11**, 371 (1979).
[13] E. B. V. Dussan, E. Ramé, and S. Garoff, J. Fluid Mech. **230**, 97 (1991).
[14] J. Koplik, J. R. Banavar, and J. F. Willemsen, Phys. Rev. Lett. **60**, 1282 (1988).
[15] P. A. Thompson and M. O. Robbins, Phys. Rev. Lett. **63**, 766 (1989).
[16] T. Z. Qian, X.-P. Wang, and P. Sheng, Phys. Rev. Lett. **93**, 094501 (2004).
[17] R. Kubo, Rep. Prog. Phys. **29**, 255 (1966).
[18] X.-M. Xiong, S. Guo, Z.-L. Xu, P. Sheng, and P. Tong, Phys. Rev. E **80**, 061604 (2009).
[19] H.-L. Ma, J. Jimenez, and R. Rajagopalan, Langmuir **16**, 2254 (2000).
[20] See Supplemental Material, Sec. I Experiment at http://link.aps.org/supplemental/10.1103/PhysRevLett.111.026101 for more details.
[21] L. D. Landau and E. M. Lifshitz, *Fluid Mechanics* (Butterworth-Heinemann, Oxford, 1986), 2nd ed.
[22] T. Z. Qian, X.-P. Wang, and P. Sheng, Phys. Rev. E **68**, 016306 (2003).
[23] T. Z. Qian, X.-P. Wang, and P. Sheng, J. Fluid Mech. **564**, 333 (2006).
[24] W. E. Williams, J. Fluid Mech. **25**, 589 (1966).
[25] W. Zhang and H. A. Stone, J. Fluid Mech. **367**, 329 (1998).
[26] M. Loewenberg, Phys. Fluids A **5**, 3004 (1993).
[27] See Supplemental Material, Sec. III Data Analysis at http://link.aps.org/supplemental/10.1103/PhysRevLett.111.026101 for more details.
[28] See Supplemental Material, Sec. IV Contact Line Dissipation in a Thin Soap Film at http://link.aps.org/supplemental/10.1103/PhysRevLett.111.026101 for more details.
[29] See Supplemental Material, Sec. II Direct Numerical Simulation at http://link.aps.org/supplemental/10.1103/PhysRevLett.111.026101 for more details.
[30] M. Gao and X.-P. Wang, J. Comput. Phys. **231**, 1372 (2012).